Princeton Plasma Physics Laboratory

PPPL-5300

Laser Pulse Compression Using Magnetized Plasmas

Y. Shi, H. Qin, N. Fisch

September 2016

PPPL PRINCETON PLASMA PHYSICS LABORATORY

Prepared for the U.S.Department of Energy under Contract DE-AC02-09CH11466.

Princeton Plasma Physics Laboratory
Report Disclaimers

Full Legal Disclaimer

Trademark Disclaimer

PPPL Report Availability

Princeton Plasma Physics Laboratory:

http://www.pppl.gov/techreports.cfm

Office of Scientific and Technical Information (OSTI):

http://www.osti.gov/scitech/

Related Links:

U.S. Department of Energy

U.S. Department of Energy Office of Science

U.S. Department of Energy Office of Fusion Energy Sciences

Laser Pulse Compression Using Magnetized Plasmas

Yuan Shi,[1,2,*] Hong Qin,[1,2,3] and Nathaniel J. Fisch[1,2]

[1]*Department of Astrophysical Sciences, Princeton University, Princeton, NJ 08544 USA*
[2]*Princeton Plasma Physics Laboratory, Princeton University, Princeton, NJ 08543 USA*
[3]*School of Nuclear Science and Technology, University of Science and Technology of China, Hefei, Anhui 230026, China*

(Dated: September 2, 2016)

Efficient pulse compression using Raman or Brillouin backscattering in unmagnetized plasma is possible only within a window in the laser intensity-frequency space. This window can be expanded by applying an external magnetic field transverse to the direction of laser propagation. Adding the transverse magnetic field enables the use of higher frequency or lower intensity pumps, producing output pulses at possibly higher intensities and longer durations. The technological challenge in this technique lies in producing the requisite strong magnetic field. However, this replaces the possibly more difficult technological challenge in producing high-density uniform plasma.

Hitherto, waves considered for mediating intense pulse compression in plasmas were the Langmuir wave and the ion acoustic wave [1–3]. However, by introducing external magnetic fields, more waves become available. Those that can be utilized for pulse compression are the electrostatic waves, including electron-motion dominant upper-hybrid wave and electron Bernstein waves, as well as ion-motion dominant Alfv́en waves, lower-hybrid waves, and ion Bernstein waves. In resonances provided by these waves, contributions from plasma density and temperature are partially replaced by more controllable contributions from external magnetic fields. This alleviates many deleterious effects [4], making it possible to expand the operation window of plasma pulse compression, producing output pulses at higher intensities.

Here, we examine pulse compression mediated by the upper-hybrid (*UH*) wave in the case where the lasers propagate perpendicular to the external magnetic field. This configuration is particularly easy to set up experimentally, where it is demanded that the amplified pulse be focused onto some target (see Fig. 1). When propagating perpendicular to the external magnetic field [5], one electromagnetic eigenmode is the O wave, whose electric field is parallel to the external magnetic field, with the ordinary dispersion relation $n_\perp^2 = 1 - \omega_p^2/\omega^2$. Here, $n_\perp = ck_\perp/\omega$ is the refractive index and ω_p is the plasma frequency. The other electromagnetic eigenmode is the X wave, which hybridizes with the electrostatic eigenmode, the *UH* wave, by the dispersion relation $n_\perp^2 = RL/S$. Here, $R, L = 1 - \omega_p^2/[\omega(\omega \pm \Omega)]$, respectively, and $S = (R + L)/2$, where $\Omega = eB_0/m_e$ is the electron gyrofrequency. The electric field of the X wave or the *UH* wave is in the plane perpendicular to the magnetic field, and spans an angle ϕ with respect to the wave vector, with $\tan\phi = S/D$, where $D = (R - L)/2$.

In the fluid regime, where the laser wavelength is larger than the Debye length λ_D and the photon density n_γ is much higher than the electron density n_e, the coupling between the pump laser (with frequency ω_1) and the seed pulse (with frequency ω_2) through the mediating *UH* wave can be well described by the classical three-wave equations. Denote $\omega_0 = \omega_1 \simeq \omega_2$ the frequency of the lasers, and $\omega_3 = \sqrt{\omega_p^2 + \Omega^2}$ the frequency of the *UH* wave. Using three-wave resonance conditions, it can be shown that in the limit $\omega_0 \gg \omega_3$, the electromagnetic eigenmodes are transverse with little dispersion, and the *UH* wave is almost longitudinal with approximately zero group velocity. Consequently, the three-wave interaction in the magnetized case has one-to-one correspondence with that in the unmagnetized case:

$$\begin{aligned}(\partial_t + c\partial_x)a_1 &= \frac{\omega_p}{2}a_2 a_3,\\ (\partial_t - c\partial_x)a_2 &= -\frac{\omega_p}{2}a_1 a_3^*,\\ \partial_t a_3 &= -\frac{\omega_0\omega_p}{2\omega_3}a_1 a_2^*.\end{aligned} \tag{1}$$

Here, the electric field amplitude of the pump and the seed are normalized by $a_{1,2} = eE_{1,2}/m_e c\omega_{1,2}$, respectively, and $a_3 = eE_3/m_e c\omega_p$ is the normalize amplitude of the *UH* wave. While an X wave and an O wave do not couple, two X waves or two O waves couple in the same way, which is described by the above equations. In the linear stage of the amplification, where pump depletion is negligible, the growth rate is

$$\Gamma_R = \frac{\sqrt{\omega_3\omega_0}}{2}|a_1|\gamma_B^{-1}. \tag{2}$$

Here, $\gamma_B := \omega_3/\omega_p > 1$ measures the extent to which plasma density is replaced by magnetic field in the *UH* resonance. In the limit where the magnetic field goes to zero, γ_B goes to 1, and the *UH* wave recovers the Langmuir wave. Governed by the same three-wave equation, the pulse compression process in the magnetized case is the same as that in the unmagnetized cases. However, physical processes that limit pulse compression are different. In what follows, we discuss the essential differences.

First, the maximum pump intensity that can be used for amplifying the pulse is limited by wavebreaking. In magnetized plasmas, the wavebreaking intensity is modified by the Lorentz force [6]. The *UH* wave breaks when the electron quiver velocity in the $\mathbf{k}_3$-direction

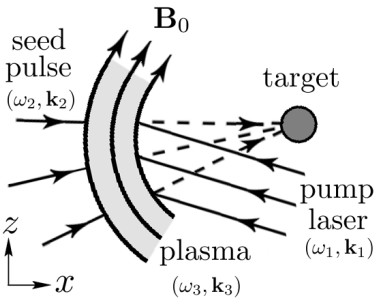

FIG. 1. A schematic drawing for amplifying and focusing a seed pulse by stimulated backscattering of a pump laser in magnetized plasma.

$v_q \simeq eE_3\omega_3/m_e\omega_p^2$ exceeds the wave phase velocity $v_p = \omega_3/k_3 \simeq c\omega_3/2\omega_0$. The condition $v_q \lesssim v_p$, which guarantees that the *UH* wave remains unbroken, can be written in terms of a_3 as $|a_3| \lesssim \omega_3/2\omega_0\gamma_B$. Using the Manley-Rowe relation, the maximum amplitude of the *UH* wave $|a_3| \leq \sqrt{\omega_0/\omega_3}|a_1|$, so a sufficient condition that the *UH* wave remains unbroken during the pulse compression process can be written in terms of a constraint on the pump intensity $I_1 = 8I_c|a_1|^2$ as

$$I_1 \lesssim I_c\Big(\frac{\omega_3}{\omega_0}\Big)^3\gamma_B^{-2}. \tag{3}$$

Here, $I_c = n_c m_e c^3/16$, and $n_c = \epsilon_0 m_e\omega_0^2/e^2$ is the critical density. When more plasma density is replaced by magnetic field in ω_3, less energy can be contained in the *UH* wave, giving rise to the γ_B^{-2} reduction. For given laser parameters, the wavebreaking constraint imposes limits on the minimum plasma density, as well as the maximum magnetic field.

Second, the maximum time that the pulse can be amplified inside the pump is limited by instabilities. The fastest growing instability is the modulational instability [1, 4], whose growth rate is reduced to

$$\Gamma_M = \frac{\omega_3^2}{8\omega_0}|a|^2\gamma_B^{-2}, \tag{4}$$

when plasma density is replaced by magnetic field. Since $\Gamma_M \ll \Gamma_R$ even at the wavebreaking intensity, this instability does not prevent the amplification from reaching the nonlinear stage, which can continue until

$$t_M \approx (12\delta\Lambda_0^2)^{1/3}\frac{\gamma_B^{4/3}}{\omega_3 a_{10}^{4/3}}. \tag{5}$$

Here, $\delta = \int\Gamma_M dt \sim 1$ is the accumulated phase shift, Λ_0 is the number of linear exponentiations before the nonlinear stage is reached, and a_{10} is the initial pump amplitude. The highest pulse compression is attained at this maximum compression time. The combination of larger t_M but smaller Γ_R in magnetized plasmas results in leading spike intensity $I_2 \approx 16I_c(3\delta/\Lambda_0)^{2/3}(2a_{10})^{4/3}\gamma_B^{2/3}\omega_0/\omega_3$, and duration $\Delta t_2 \approx 2(2\Lambda_0/3\delta)^{1/3}a_{10}^{-2/3}\gamma_B^{2/3}/\omega_0$. Ramping up the pump intensity while keeping plasma parameters fixed, the maximum output intensity is reached using the most intense pump allowed by wavebreaking, which gives $I_2 \leq 16I_c(3\delta/2\Lambda_0)^{2/3}\gamma_B^{-2/3}\omega_3/\omega_0$. On the other hand, optimizing plasma parameters while keeping lasers fixed, the maximum output intensity is reached using the smallest possible ω_3 allowed by wavebreaking, which gives $I_2 \leq 8I_c(3\delta a_{10}/2\Lambda_0)^{2/3}$, independent of γ_B. This output intensity could be achieved using unmagnetized plasmas, if wavebreaking and longitudinal modulational instability were the only limiting effects.

Third, the *UH* wave is damped collisionlessly. Although the *UH* wave is linearly undamped when propagating exactly perpendicular to the magnetic field [5, 7], it is nevertheless damped nonlinearly due to surfatron acceleration of trapped particles parallel to the wave front [8], as well as stochastic heating of untrapped particles when the wave amplitude is above threshold [9]. For the *UH* wave, the wave frequency is typically comparable to the gyrofrequency. If an electron has perpendicular velocity close to v_p, the phase velocity of the wave, it sees an almost constant electric field. The electron may gain or loss energy to the wave, depending on the relative phase of wave motion and gyromotion. The phase mixing process causes the *UH* wave to damp on a Maxwellian background with rate $\nu_L \approx \sqrt{\pi}(v_p/v_T)^3\exp(-v_p^2/v_T^2)\omega_p^2/\omega_3$, where v_T is te thermal velocity. Since the bulk of the distribution needs to support the linear wave in the first place, it is necessary that $v_p > v_T$. So the condition that collisionless damping is weak may be approximated as

$$\frac{\nu_L}{\omega_3} \approx \sqrt{\pi}(3/2)^{3/2}e^{-v_p^2/v_T^2}\gamma_B^{-2} \ll 1. \tag{6}$$

As $\omega_3 \to |\Omega|$, the electron density vanishes, so there are few electrons to participate in phase mixing, and collisionless damping diminishes consequently.

Fourth, both lasers and *UH* wave are damped collisionally. Suppose the electron quiver motion is randomized by one electron-ion collision, during which the fraction of wave energy carried by particles is completely thermalized, then the collisional damping rate of of the *UH* wave and lasers can be estimated by $\nu_3 \approx \nu_{ei}(1-\omega_p^2/2\omega_3^2)$ and $\nu_0 \approx \nu_{ei}\omega_p^2/2\omega_0^2$, respectively. Here, the electron-ion collision frequency $\nu_{ei} \approx n_e Z^2 e^4\Lambda/(4\pi\epsilon_0)^2 m_e^2 v^3$, where Z is the ion charge, Λ is the Coulomb logarithm, and v is the characteristic velocity of electrons with respect to the ion background. The velocity v contains contributions from both thermal motion and wave motion. By ignoring the contribution from wave motion, an upper bound of the collision frequency can be estimated. To mediate efficient energy transfer, the *UH* wave must remain weakly damped during the seed transient time on the order of Δt_2. To penetrate the plasma, the laser damping time

must be larger than the average pulse amplification time $t_M/2$. Hence, the conditions that collision damping are weak can be written as

$$\nu_3 \Delta t_2 \lesssim 1, \quad \nu_0 t_M/2 \lesssim 1. \tag{7}$$

The above constraints are more strict than $\nu_0\nu_3 < \Gamma_R^2$, the condition that parametric instability can be excited by the pump, when $\Lambda_0 \geq 2$. By replacing electron density with magnetic field in ω_3, the constraints imposed by collisional damping of the *UH* wave and the lasers are alleviated by $\gamma_B^{-4/3}$ and $\gamma_B^{-8/3}$, respectively, if pulse compression uses the maximum time allowed by the modulation instability. When less amplification time is used, the pulse duration becomes longer. In this case, the constraint imposed by collisional damping is more strict for the *UH* wave and less strict for the lasers. Due to the reduction of the wave damping, the fluence of the output pulse is larger at fixed pump fluence, which can be advantageous in many applications.

The four physical limits discussed above, together with fluid model constraints, define a window within which efficient pulse compression is possible. Adding a magnetic field enables improvement of this window by providing an extra adjustable parameter γ_B. The first improvement comes from the expansion of the operation window. For a given laser frequency ω_0 and pump intensity I_1, efficient pulse compression is possible if there exist n_e, T_e, and B_0, such that all constraints are satisfied. For the sake of illustration, let us replace conditions of the type $x \ll y$ by more quantitative conditions of the type $x/y < 0.1$, which set the Manley-Rowe efficiency at 90%. When projected in the ω_0-I_1 space, the resultant operation windows are the colored regions enclosed by black boundaries in Fig. 2, for unmagnetized case (a) and magnetized case (b), if hydrogen plasmas are used. Above AB and BB', the wavebreaking limit is exceeded while keeping $\omega_3 \ll \omega_0$. To the right of BC or B'C', efficient pulse compression might still be possible, but then collisionless damping becomes strong while keeping $n_e\lambda_D^3 \gg 1$. Below CD or C'D', either collisional damping or collisionless damping becomes strong while keeping $n_\gamma \gg n_e$ and $n_e\lambda_D^3 \gg 1$. The alleviation of the modulational instability and the wave damping in the magnetized case gives rise to the second improvement, which is the possibility of intensifying the output pulses. In Fig. 2a, we plot the ratio of the maximum achievable output intensity in the magnetized case I_2^m versus that in the unmagnetized case I_2^u in color scale. As a reference, we plot I_2^m/I_1 in (b). The third improvement comes from the technological advantage of replacing plasma density with magnetic field, whose strength and uniformity is much more controllable experimentally. The plasma density, in the units of $10^{20}\,\mathrm{cm}^{-3}$, needed for achieving I_2^u and I_2^m are plotted by dashed contours in (a) and (b), respectively. Apparently, the necessary density in the magnetized case is less than that in the unmagnetized case. In (b), we also plot the minimum magnetic field necessary for achieving I_2^m using solid contours. As expected, the external magnetic field has appreciable effect when it is larger than the laser magnetic field.

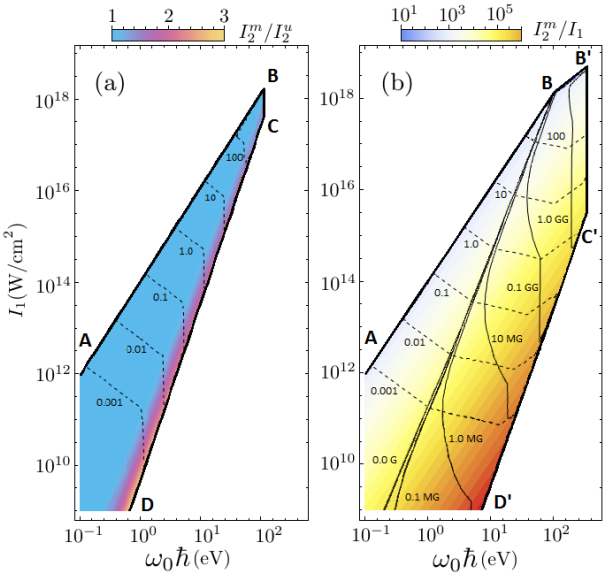

FIG. 2. Operation windows of efficient pulse compression using hydrogen plasmas. (a) $B_0 = 0$. The color scale is the ratio of the maximum output intensity achievable in the magnetized case I_2^m versus that in the unmagnetized case I_2^u. The dashed contours are plasma density necessary for achieving I_2^u. (b) $B_0 \geq 0$. The color scale is the ratio I_2^m/I_1. The dashed contours are plasma density necessary for achieving I_2^m, and the solid contours are the minimum necessary magnetic field. Plasma density is in the units of $10^{20}\,\mathrm{cm}^{-3}$.

To give an example where unmagnetized compressors can work but magnetized compressors can work better, consider compression of KrF laser pulses. For example, KrF pulses produced at the Nike laser facility have kilojoules in energy with nanoseconds durations [10]. These pulses can be focused on a spot of size $\sim 0.01\mathrm{cm}^2$, reaching peak intensity $\sim 10^{14}\mathrm{W/cm}^2$. The average intensity, however, falls in the range $10^{12} - 10^{13}\mathrm{W/cm}^2$. Since the photon energy of the KrF laser is ~ 5 eV, the unmagnetized operation window (Fig. 2a) is about to close when the laser intensity is at the lower end. In Fig. 3a, we plot the operation windows projected in the T_e-n_e space for hydrocarbon plasmas (C_3H_8, $Z_{\mathrm{eff}} \approx 2.36$) when $I_1 = 10^{13}$ W/cm^2. Efficient compression can be achieved using plasmas whose temperature and density are within the windows. As can be seen from the figure, the narrow unmagnetized window can be expanded by applying a 5-megagauss external magnetic field. The requisite minimum plasma density is reduced to $n_e \approx 0.35 \times 10^{19}\mathrm{cm}^{-3}$, corresponding to $\gamma_B \approx 1.3$. Suppose the initial seed intensity is such that $\Lambda_0 \approx 6$, then the maximum amplification time is $t_M \approx 1.3$ ns, within which as large as

$\sim$ 321 linear exponentiations could be made. The output pulse has intensity $I_2 \approx 2.7 \times 10^{17}\mathrm{W/cm}^2$ and duration $\Delta t_2 \approx 65$ fs. The efficiency of compression is about 67.5%. In comparison, using an unmagnetized plasma, the requisite density is as least $n_e \approx 0.85 \times 10^{19}\mathrm{cm}^{-3}$, which gives $t_M \approx 0.8$ ns, $I_2 \approx 1.9 \times 10^{17}\mathrm{W/cm}^2$, and $\Delta t_2 \approx 54$ fs, with $\sim 64.1\%$ efficiency.

To give an example where magnetized compressors can work whereas unmagnetized compressors cannot, consider compression of soft x ray pulses. For example, pulses produced at the Linac Coherent Light Source have $2-6$ mJ in energy, $5-500$ fs in duration, and focal spot size $\sim 10\ \mu\mathrm{m}^2$ [11]. These correspond to a laser intensity $\sim 10^{18}$ W/cm^2. Since photons in these pulses have energy in the range 250 eV $-$ 10 KeV, pulse compression using unmagnetized plasmas (Fig. 2) may only be achieved inefficiently [12]. However, by applying a magnetic field on the order of gigagauss, efficient compression can be made possible. The operation window projected in the T_e-n_e space is plotted in Fig. 3b, for the case $I_1 = 10^{18}$ W/cm^2, $\omega_0\hbar = 250$ eV, and $B_0 = 1.5$ GG, using a hydrogen plasma. The maximum compression is achieved at the lowest density $n_e \approx 7.93 \times 10^{22}\mathrm{cm}^{-3}$, corresponding to $\gamma_B \approx 1.9$. Suppose $\Lambda_0 \approx 6$, then the modulational instability limits the maximum amplification length to be $t_M c \approx 0.26$ mm, corresponding to a pump duration of ~ 1.7 ps. Within this time, ~ 82 linear exponentiations could be made, so the pulse compression can develop well into the nonlinear stage. The output pulse intensity is $I_2 \approx 2.3 \times 10^{21}\mathrm{W/cm}^2$ with duration $\Delta t_2 \approx 0.5$ fs. In this example, the pulse compression ratio is about a thousand with $\sim 67.6\%$ efficiency.

To achieve pulse compression experimentally, it is necessary to produce plasma targets with specific density and temperature. Moreover, in order to resonantly couple the pump with the seed, these targets must have appropriate geometry and uniformity. Unmagnetized targets satisfying these requirements are in principle attainable but in practice challenging. The laboratory standard is to ionize a gas jet [13]. This is appropriate for plasma targets with density less than $10^{20}\mathrm{cm}^{-3}$, temperature $\sim 10^1$ eV, and size on the order of millimeter. Producing unmagnetized targets of even higher density has been envisioned using a dense aerosol jet [14], but reaching high temperature and necessary uniformity with these targets is yet to be demonstrated experimentally.

Using magnetized plasmas, the challenge in producing high density uniform plasmas is replaced by the challenge in producing strong uniform magnetic fields, for which the technology is already within reach. One technique uses capacitor-coil targets driven by intense lasers. In a number of experiments [15], generation of megagauss magnetic field, which is uniform on millimeter scale and quasi-static on nanosecond scale, has been demonstrated. Another technique uses planar solid targets ablated by intense laser pulses [16]. This technique has successfully

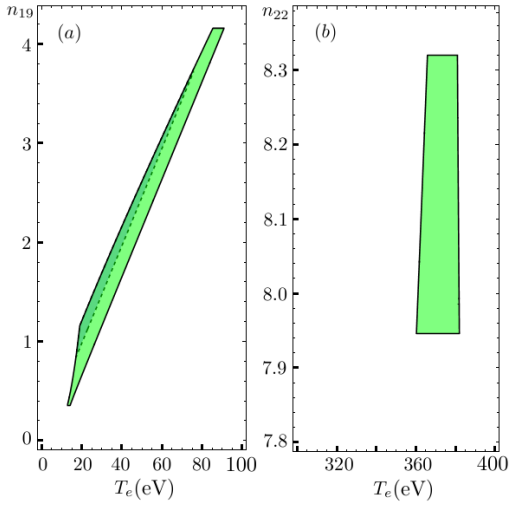

FIG. 3. Operation windows in plasma parameter space. The green regions enclosed in solid lines are the magnetized windows, and the blue region enclosed in the dashed lines is the unmagnetized window. The left boundaries are due to collisional damping; the right boundaries are due to collisionless damping; the upper boundaries are required by $\omega_3 \ll \omega_0$ and $n_e \ll n_\gamma$; and the bottom boundaries are due to wavebreaking. (a) KrF laser with $I_1 = 10^{13}$ W/cm^2 and $\omega_0\hbar = 5$ eV. n_e is in the units of $10^{19}\mathrm{cm}^{-3}$. $B_0 = 5$ MG. (b) Soft x ray laser with $I_1 = 10^{18}$ W/cm^2 and $\omega_0\hbar = 250$ eV. n_e is in the units of $10^{22}\mathrm{cm}^{-3}$. $B_0 = 1.5$ GG.

produced plasmas with $\sim 10^{21}\mathrm{cm}^{-3}$ density and magnetic fields on the order of gigagauss, when picoseconds pulses with ~ 1 μm wavelength and $\sim 10^{20}\mathrm{W/cm}^2$ intensity are used for ablation. The density and magnetic field produced near the solid surfaces are uniform on micrometer scale and quasi-static on picosecond scale. Improving laser platforms such that magnetized plasma targets are improved by one to two orders of magnitude in density and uniformity will make efficient compression of powerful soft x-ray lasers possible.

To summarize, the techniques explored here may enable compression of powerful lasers beyond the reach of the currently envisioned methods using unmagnetized plasmas. By substituting the requirement for high plasma density with one for an external magnetic field, the mediating wave is then the upper hybrid wave rather than the Langmuir wave. Deleterious physical effects associated with high plasma density are then alleviated and the engineering requirements of producing high and uniform plasma densities can be relaxed. Thus, using magnetized plasmas, the operation window might be significantly expanded, with efficient pulse compression achievable both for higher frequency and lower intensity pump lasers, with the possibility of producing output pulses of both higher intensity and longer duration.

The work is supported by NNSA Grant No. DE-NA0002948, AFOSR Grant No. FA9550-15-1-0391, and DOE Research Grant No. DEAC02-09CH11466.

* yshi@pppl.gov

[1] R. D. Milroy, C. E. Capjack, and C. R. James, Phys. Fluids **22**, 1922 (1979); C. E. Capjack, C. R. James, and J. N. McMullin, J. Appl. Phys. **53**, 4046 (1982); V. M. Malkin, G. Shvets, and N. J. Fisch, Phys. Rev. Lett. **82**, 4448 (1999).

[2] A. A. Andreev, C. Riconda, V. T. Tikhonchuk, and S. Weber, Phys. Plasmas **13**, 053110 (2006); S. Weber, C. Riconda, L. Lancia, J.-R. Marquès, G. A. Mourou, and J. Fuchs, Phys. Rev. Lett. **111**, 055004 (2013); A. Frank, J. Fuchs, L. Lancia, G. Lehmann, J.-R. Marquès, G. Mourou, C. Riconda, K. Spatschek, T. Toncian, L. Vassura, and S. Weber, Eur. Phys. J-Spec. Top. **223**, 1153 (2014); G. Lehmann and K. H. Spatschek, Phys. Plasmas **23**, 023107 (2016).

[3] C. Riconda, S. Weber, L. Lancia, J.-R. Marqus, G. A. Mourou, and J. Fuchs, Physics of Plasmas **20**, 083115 (2013); Q. Jia, I. Barth, M. R. Edwards, J. M. Mikhailova, and N. J. Fisch, *ibid.* **23**, 053118 (2016).

[4] D. S. Clark and N. J. Fisch, Phys. Plasmas **10**, 3363 (2003); V. M. Malkin, N. J. Fisch, and J. S. Wurtele, Phys. Rev. E **75**, 026404 (2007); V. M. Malkin and N. J. Fisch, Eur. Phys. J-Spec. Top. **223**, 1157 (2014).

[5] T. Stix, *Waves in Plasmas* (American Inst. of Physics, 1992).

[6] M. Karmakar, C. Maity, and N. Chakrabarti, Phys. Plasmas **23**, 064503 (2016).

[7] A. I. Sukhorukov and P. Stubbe, Phys. Plasmas **4**, 2497 (1997).

[8] R. Sagdeev and V. Shapiro, JETP Lett. **17**, 279 (1973); J. M. Dawson, V. K. Decyk, R. W. Huff, I. Jechart, T. Katsouleas, J. N. Leboeuf, B. Lembege, R. M. Martinez, Y. Ohsawa, and S. T. Ratliff, Phys. Rev. Lett. **50**, 1455 (1983).

[9] C. F. F. Karney, Phys. Fluids **21**, 1584 (1978); **22**, 2188 (1979).

[10] S. P. Obenschain, S. E. Bodner, D. Colombant, K. Gerber, R. H. Lehmberg, E. A. McLean, A. N. Mostovych, M. S. Pronko, C. J. Pawley, A. J. Schmitt, J. D. Sethian, V. Serlin, J. A. Stamper, C. A. Sullivan, J. P. Dahlburg, J. H. Gardner, Y. Chan, A. V. Deniz, J. Hardgrove, T. Lehecka, and M. Klapisch, Phys. Plasmas **3**, 2098 (1996).

[11] C. Bostedt, J. D. Bozek, P. H. Bucksbaum, R. N. Coffee, J. B. Hastings, Z. Huang, R. W. Lee, S. Schorb, J. N. Corlett, P. Denes, P. Emma, R. W. Falcone, R. W. Schoenlein, G. Doumy, E. P. Kanter, B. Kraessig, S. Southworth, L. Young, L. Fang, M. Hoener, N. Berrah, C. Roedig, and L. F. DiMauro, J. Phys. B-At. Mol. Opt. **46**, 164003 (2013).

[12] J. D. Sadler, R. Nathvani, P. Olekiewicz, L. A. Ceurvorst, N. Ratan, M. F. Kasim, R. M. G. M. Trines, R. Bingham, and P. A. Norreys, Sci, Rep. **5**, 16755 (2015).

[13] Y. Ping, W. Cheng, S. Suckewer, D. S. Clark, and N. J. Fisch, Phys. Rev. Lett. **92**, 175007 (2004); W. Cheng, Y. Avitzour, Y. Ping, S. Suckewer, N. J. Fisch, M. S. Hur, and J. S. Wurtele, **94**, 045003 (2005); L. Lancia, J.-R. Marquès, M. Nakatsutsumi, C. Riconda, S. Weber, S. Hüller, A. Mančić, P. Antici, V. T. Tikhonchuk, A. Héron, P. Audebert, and J. Fuchs, **104**, 025001 (2010); L. Lancia, A. Giribono, L. Vassura, M. Chiaramello, C. Riconda, S. Weber, A. Castan, A. Chatelain, A. Frank, T. Gangolf, M. N. Quinn, J. Fuchs, and J.-R. Marquès, **116**, 075001 (2016).

[14] M. J. Hay, E. J. Valeo, and N. J. Fisch, Phys. Rev. Lett. **111**, 188301 (2013); D. Ruiz *et al.*, Journal of Aerosol Science **76**, 115 (2014).

[15] S. Fujioka *et al.*, Sci, Rep. **3**, 1170 (2013); J. J. Santos *et al.*, New J. Phys. **17**, 083051 (2015).

[16] U. Wagner, M. Tatarakis, A. Gopal, F. N. Beg, E. L. Clark, A. E. Dangor, R. G. Evans, M. G. Haines, S. P. D. Mangles, P. A. Norreys, M.-S. Wei, M. Zepf, and K. Krushelnick, Phys. Rev. E **70**, 026401 (2004); M. Tatarakis *et al.*, Phys. Plasmas **9**, 2244 (2002); M. Borghesi, A. J. MacKinnon, A. R. Bell, R. Gaillard, and O. Willi, Phys. Rev. Lett. **81**, 112 (1998).

PPPL PRINCETON PLASMA PHYSICS LABORATORY

Princeton Plasma Physics Laboratory
Office of Reports and Publications

Managed by
Princeton University

under contract with the
U.S. Department of Energy
(DE-AC02-09CH11466)

P.O. Box 451, Princeton, NJ 08543
Phone: 609-243-2245
Fax: 609-243-2751

E-mail: publications@pppl.gov

Website: http://www.pppl.gov